Ocean Modelling 38 (2011) 251–266

Contents lists available at ScienceDirect

Ocean Modelling

journal homepage: www.elsevier.com/locate/ocemod

Predicting the East Australian Current

Terence J. O'Kane [a,*], Peter R. Oke [a], Paul A. Sandery [b]

[a] CSIRO Marine & Atmospheric Research, Hobart, Australia
[b] Bureau of Meteorology, Melbourne, Australia

ARTICLE INFO

Article history:
Received 7 April 2010
Received in revised form 14 January 2011
Accepted 4 April 2011
Available online 12 April 2011

Keywords:
Ocean forecasting
Ensemble prediction
East Australian Current

ABSTRACT

Results are presented from an ensemble prediction study (EPS) of the East Australian Current (EAC) with a specific focus on the examination of the role of dynamical instabilities and flow dependent growing errors. The region where the EAC separates from the coast, is characterized by significant mesoscale eddy variability, meandering and is dominated by nonlinear dynamics thereby representing a severe challenge for operational forecasting. Using analyses from OceanMAPS, the Australian operational ocean forecast system, we explore the structures of flow dependent forecast errors over 7 days and examine the role of dynamical instabilities. Forecast ensemble perturbations are generated using the method of bred vectors allowing the identification of those perturbations to a given initial state that grow most rapidly. We consider a 6 month period spanning the Austral summer that corresponds to the season of maximum eddy variability. We find that the bred vector (BV) structures occur in areas of instability where forecast errors are large and in particular in regions associated with the Tasman Front and EAC extension. We also find that very few BVs are required to identify these regions of large forecast error and on that basis we expect that even a small BV ensemble would prove useful for adaptive sampling and targeted observations. The results presented also suggest that it may be beneficial to supplement the static background error covariances typically used in operational ocean data assimilation systems with flow dependent background errors calculated using a relatively cheap EPS.

1. Introduction

Ocean forecasting has seen major advances in the past decade. Many countries now perform operational forecasts of the mesoscale ocean circulation (see Hurlburt et al., 2009 and references therein). Many of the advances in ocean forecasting are on the back of numerical weather prediction (NWP), particularly those in data assimilation (Cummings et al., 2009). Ocean forecasting is underpinned by satellite observations of sea-level anomalies (SLA) and sea-surface temperature (SST), and in situ observations from Argo floats and a sparse array of tropical moorings (Oke et al., 2009). The most energetic scales of the oceans are in the mesoscale, which is characterized by eddies and meanders, and occurs particularly in western boundary current (WBC) regions. These scales are only marginally resolved by the above-mentioned components of the global ocean observing system. As a result, we expect the errors of operational ocean forecasts to be variable in time. The errors of the day are likely to depend on the coverage of assimilated observations and the stability of the ocean's circulation. For atmospheric flows synoptic-scale forecast errors over the extra-tropics are known to be dominated by the amplification of errors in specifying the initial state whereas forecast errors in the tropics are largely influenced by model error i.e. physics parameterizations. The respective roles of model and initialization errors in ocean forecasting remains a largely open question.

One of the most difficult problems in NWP is to predict regime transitions associated with rapidly growing dynamic instabilities such as those associated with mid-latitude blocking regime transitions (O'Kane and Frederiksen, 2008a). Currently the dominant approaches to ensemble prediction (EP) for synoptic scale weather are based on generating an ensemble of deterministic forecasts whose differences are perturbation vectors, centered about an unperturbed or control forecast. The initial perturbation vectors are typically chosen to capture flow dependent information about the deterministic chaotic system (Pazó et al., 2010). Operational EP systems include those based on singular vectors (Molteni et al., 1996), bred vectors (Tracton and Kalnay, 1993; Toth and Kalnay, 1997) or generalizations of bred vectors such as the ensemble transform (ET) (Wei et al., 2008) and the ensemble transform Kalman filter (ETKF) (Bowler et al., 2009; Wei et al., 2006; O'Kane et al., 2008).

Several data assimilation approaches use ensembles to model the time-evolving background error covariance (Evensen, 2003). These approaches generally require a modest-sized ensemble to reliably represent the background error covariance. If the ensemble is too small, the ensemble is likely to be dominated by sampling error, and the ensemble-based covariance will be corrupted by noise.

* Corresponding author. Tel.: +61 3 62325066; fax: +61 3 62325123.
E-mail address: terence.okane@csiro.au (T.J. O'Kane).

1463-5003/$ - see front matter
doi:10.1016/j.ocemod.2011.04.003

Localization (Houtekamer and Mitchell, 1998) can be employed to reduce the sampling error, but this is not an ideal solution because it can result in the introduction of dynamical imbalance that can degrade the model's performance (Mitchell et al., 2002).

The typical ensemble size needed to model a system's time-evolving background error covariance can be impractical, due to the significant computational requirements. Instead, we seek to explore the possibility of using a very small ensemble of bred vectors (Toth and Kalnay, 1993; Toth and Kalnay, 1997) to qualitatively represent the errors of the day. Bred, Lyapunov and Singular vectors (to the tangent linear operator) (Trevisan and Pancotti, 1998; Pazó et al., 2010) may all be applied to identify the spatial structures of a system's fastest growing modes. Toth and Kalnay (1997) suggest that a systems bred vectors, nonlinear finite amplitude local generalizations of the leading Lyapunov vectors, should have similar structures to the systems background errors. Corazza et al. (2003) presented results to support this conjecture for an atmospheric application using an idealized quasi-geostrophic model. We seek to further examine this idea for an oceanographic case study using an ocean general circulation model. Specifically, we hypothesize that the bred vectors from a small ensemble size (we start with a 4-member ensemble) can provide useful prognostic information about where regions of large forecast or background errors may occur. We seek to determine whether we can use bred vectors to identify when and where instabilities are likely to occur in the ocean; and so-doing identify when and where the forecast skill of an operational ocean forecast system is likely to be low. To this end we develop a breeding system for a regional ocean model of the Tasman Sea (Fig. 1).

The main features of the Tasman Sea are the EAC and its eddies. At any point in time, the EAC is typically characterized by a narrow, strong southward flow adjacent to the continental shelf between about 15°S and 32°S. The EAC typically separates from the coast near Sugarloaf Point (SPt) (denoted in Fig. 1; Godfrey et al., 1980), forming a complicated field of warm- and cold-core eddies. Warm-core eddies are typically large, with diameters of several hundred kilometers, forming every 90 days or so (Mata et al., 2006). Cold-core eddies are smaller, perhaps 50–100 km across (e.g. Oke and Griffin, 2011), and often form at the point where the EAC separates from the coast, or on the peripheries of warm-core eddies. While warm-core eddies are usually well-resolved by altimetry, cold-core eddies are often missed. We therefore expect that forecasting the development of cold-core eddies is problematic, and is unlikely to be skillful. We seek to determine whether a breeding system can reliably and efficiently identify when and where regions of large forecast error occur and if these regions are associated with developing cold-core eddies.

This paper is organized as follows: In Section 2 we discuss the EAC dynamics and the Australian operational ocean forecast system (OceanMAPS). The ensemble prediction methodology and experimental design are described in Section 3, while the results, a discussion and conclusions are presented in Sections 4–6.

2. EAC dynamics

Part of the Western Boundary Current (WBC) system associated with the South Pacific subtropical gyre, the EAC forms near 15°S, and flows along the coast carrying on average 22 Sv ($1\ \text{Sv} = 10^6\ \text{m}^3\ \text{s}^{-1}$) attaining its maximum volume transport at 30°S (Mata et al., 2000) then tending to separate from the coast near SPt (32.5°S) (Godfrey et al., 1980) before flowing southeastward into the Tasman Sea (Wilkin and Zhang, 2007). After the EAC separates from the coast it spawns a rich field of mesoscale eddies evident in the time-mean (13 year) eddy-kinetic-energy field calculated by Schiller et al. (2008) depicted in Fig. 1. The EAC is complex and characterized by large seasonal and mesoscale variability (Ridgway and Godfrey, 1997), wind driven upwelling and eddy formation (Oke and Griffin, 2011; Roughan and Middleton, 2002) and strong eddy–eddy, eddy–mean and eddy–topographic interactions (Ridgway and Dunn, 2003). Although significantly weaker than other WBCs in terms of volume transport, the eddy variability of the EAC is comparable to the aforementioned larger Northern Hemisphere WBCs (Mata et al., 2000).

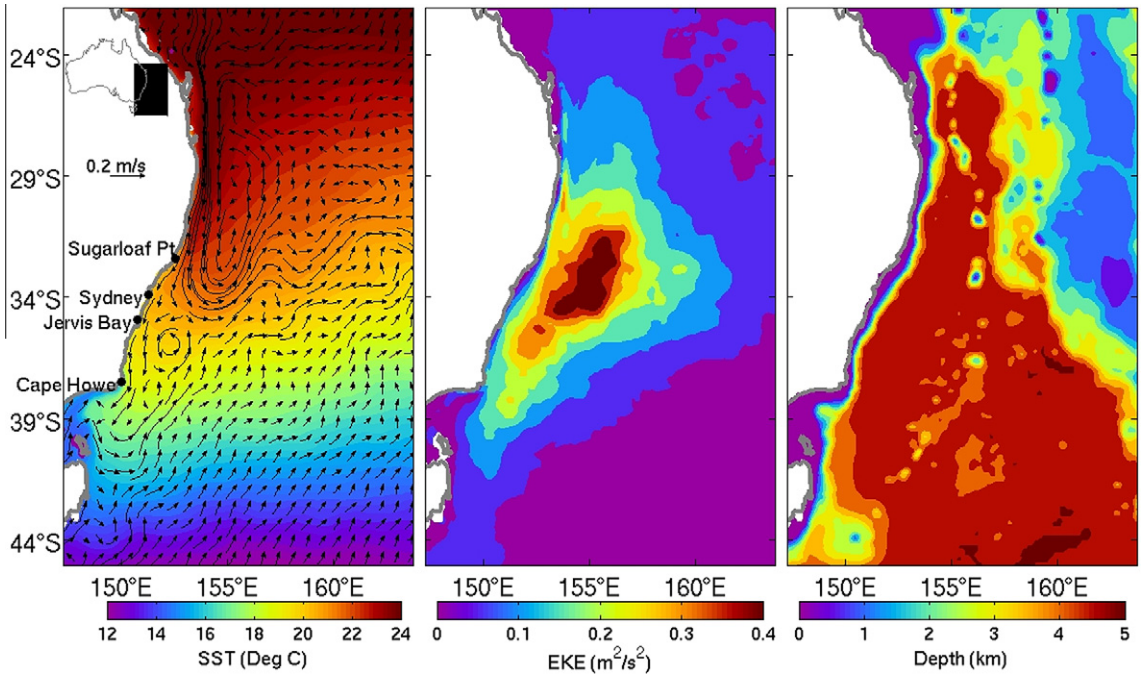

Fig. 1. Thirteen-year average (1993–2006) SST and surface velocities (left), eddy-kinetic energy (EKE; middle) computed from daily mean fields of surface velocity from BRAN2p1 (Schiller et al., 2008), and model topography (right). The inset on the left panel shows the location of the region of interest off south eastern Australia.

Early examination of oceanographic data (Godfrey et al., 1980) found the separation outflow during summer months to be typically centered on a line extending south–southeast of SPt. In winter months the total variability of the EAC was found to decrease while the region of maximum variability retreated northward as did the average separation point. More recent studies using remotely sensed data and ocean models (Mata et al., 2006; Bowen et al., 2005) characterized EAC eddy variability as originating via intrinsic instabilities of the current and that eddy shedding events occur on an ≈90 days timescale between 32°S and 35°S. Further, these events were typically preceded by a southward extension of the current beyond 32°S to as far as 34°S and that post shedding the current becomes more strongly zonal at the separation point (32°S).

Time averaged (50 days averages) modeled mean-eddy energy transfers have been used to show that while both barotropic and baroclinic instabilities are active in the retroflection region, barotropic processes tend to dominate (Mata et al., 2006). One might expect however that on much shorter timescales baroclinic instability associated with eddy formation may dominate. While the majority of previous studies of EAC mesoscale eddies have focused on warm core eddies (e.g., Andrews and Scully-Power, 1976; Nilsson and Cresswell, 1980; Brandt, 1981; Cresswell, 1982; Cresswell, 1983; Tranter et al., 1986; Huyer et al., 1988; Mata et al., 2000; Mata et al., 2006; Wilkin and Zhang, 2007), some studies have also noted the importance of cold-core eddies (e.g., Cresswell, 1974; Huyer et al., 1988; Cresswell, 1994; Gibbs et al., 1997; Oke and Griffin, 2011; Marchesiello and Middleton, 2000).

Whereas the focus of recent studies of the EAC has been on the frequency at which anticyclones pinch off from the EAC retroflection (Wilkin and Zhang, 2007; Mata et al., 2006) and the associated dynamics of the Tasman Front, our emphasis is on timescales of ≈ 1 week, that are characteristic of an operational ocean forecast systems data assimilation window. We aim to examine the predictability of the EAC mesoscale eddies and to assess whether regions of large forecast errors are associated with the rapid amplification of dynamic instability processes. The mechanisms by which local instabilities may rapidly amplify (super-Lyapunov growth) and the relationship to finite time Lyapunov and bred vectors is discussed by Trevisan and Pancotti (1998) and Pazó et al. (2010), respectively. By developing model initialization methods that incorporate flow dependencies we hope to not only better understand the EAC but to be able to better predict it.

There remain many unanswered questions regarding the mechanisms behind eddy shedding and boundary current separation in the EAC, particularly the role of instabilities and their relationship to predictability. Further there have been, to-date, no studies of the predictability of the EAC using advanced ensemble forecasting methods.

3. Ensemble prediction methodology

Early attempts at establishing the theoretical limits to predictability in the atmosphere focused on error growth using deterministic forecasts with the error determined from the divergence of pairs of initially close states (Charney, 1966; Smagorinsky, 1969; Kasahara, 1972). Later it was realized that weather forecasting could be regarded either as a statistical problem of predicting the probability density function of atmospheric states or, equivalently, of calculating the moments of meteorological variables. In order to describe the statistical behavior of a turbulent flow the underlying nonlinear dynamical equations must be averaged producing an infinite hierarchy of moment or cumulant equations. This equivalence allows one to examine ensemble prediction schemes on a fundamental level by exploiting statistical dynamical turbulence closure theory whereby prognostic equations for statistical variables are formulated (see O'Kane and Frederiksen, 2008a and references therein). Leith (1974) famously used closure theory to show that ensemble averaging acts as a nonlinear filter eliminating parts of the growing errors, provided the ensemble forecast is initialized with perturbations representative of the initial probability distribution of the basic flow about the control analysis. Toth and Kalnay (1997) demonstrated that this effect is inherent to ensemble averaging and cannot be reproduced by spatial filtering. O'Kane and Frederiksen (2008b) showed that stochastic approaches to data assimilation, like the ensemble Kalman filter, produce initial perturbations that necessarily contain both random decaying errors and dynamically generated growing errors. They developed a nonlinear statistical dynamical Kalman filter (SDKF O'Kane and Frederiksen, 2008b), based on an inhomogeneous turbulence closure, and showed how stochastic filters can suffer from introduced sampling errors leading to uncharacteristic error growth particularly during large scale atmospheric regime transitions.

3.1. General approach

The reasons that deterministic forecasts fail over reasonable prediction periods was found to be in large part due to the inherent non-linearity in the system (deterministic chaos; see Lorenz, 1963), errors in the initial conditions (analysis errors; see Cummings et al., 2009; Oke et al., 2009), model deficiencies (e.g. subgrid-scale parameterizations; see Frederiksen and O'Kane, 2008) and forcing errors. In comparison to a single control forecast, ensemble forecasts can provide not only improved estimates of the forecast (ensemble mean), but also estimates of the forecast error covariance and possibly the higher-order moments.

In this article our specific aim is to examine whether a computationally cheap ocean EPS whose initial perturbations sample only the fastest growing errors can add useful information to a deterministic ocean forecasting system. We postulate that for regions of large eddy variability, such as the EAC, forecast errors at lead times of about a week should largely arise due to local dynamic instability processes. Our approach is to periodically generate an initial analysis using an operational ocean data assimilation system. An ensemble is constructed by adding to the initial analysis finite amplitude growing perturbation vectors that are dynamically generated using the breeding technique. The ensemble, including an unperturbed control or background forecast, is then integrated forward and the evolved perturbation vectors compared to the forecast error which is taken to be the difference between the control forecast and a verifying analysis.

3.2. OceanMAPS data assimilation

The ensemble prediction studies we present in Section 4 utilize analyses provided by the Australian Bureau of Meteorology's Ocean Model Analysis and Prediction System (OceanMAPS; Brassington et al., 2006; Brassington et al., 2007; Oke et al., 2008). OceanMAPS is comprised of the Ocean Forecasting Australian Model (OFAM), based on the GFDL MOM4 code (Griffies et al., 2003), with 1/10° resolution in the region 90°E–180°E, 75°S–16°N with decreasing resolution elsewhere. OFAM is initialized by the Bluelink Ocean Data Assimilation System (BODAS; Oke et al., 2008) based on ensemble optimal interpolation (EnOI) with background error covariances defined from a stationary, or time invariant, ensemble of seasonal anomalies (72 members at present) derived from a long model integration without data assimilation. OceanMAPS uses an 11 day window of observations that include SLA from altimetry, temperature and salinity profile observations from XBT, CTD and Argo, and AMSRE SST.

3.3. Regional model and adaptive initialization

The model we use is a regional version of OFAM, based on MOM4p1 (Griffies et al., 2003) and is the ocean component of a coupled limited area model system documented by Sandery et al. (2010). It has 0.1° horizontal resolution and 47 z-levels with 10 m vertical resolution in the upper 200 m, expanding to larger spacing towards full oceanic depths. The regional model is nested inside the global model and uses sponge layer open boundary conditions for surface height η, temperature T, salinity S, and the u and v components of the velocity field, and uses the same grid and bathymetry as the global model. The domain chosen for this study covers an area in the Tasman Sea enclosed within 148.75°E–163.75°E and 45.05°S–22.05°S (see Fig. 1). The regional model is forced by surface fluxes from the Global Analysis and Spectral Model (GASP) analysis NWP cycle that is run operationally by the Australian Bureau of Meteorology (Seaman et al., 1995). A dynamical initialization scheme (Sandery and Brassington, 2009; Sandery et al., 2011) that applies time and space dependent tendency forcing as a function of differences between model and target prognostic variables is also used to maintain dynamical balance.

3.4. BV methodology

A primary aim in EPS is to generate independent initial perturbations as fast-growing disturbances with structures and growth rates typical of the analysis errors i.e. span the possible errors in the control analysis. In contrast, random initial perturbations sampled isotropically, grow more slowly and in some cases even decay leading to underestimated error variances. Additionally the computational cost of running many realizations of a high resolution model leads to severe restrictions on the number of available perturbations and so we aim to sample only the fastest growing error structures.

The method of bred perturbations allows information about the fast-growing errors to be incorporated into the initial perturbations for the forecast. For particularly dynamic flows, such as when emergent coherent structures are developing (for example atmospheric high-low blocking dipoles or eddy shedding associated with oceanic boundary current separation), errors arise due to fast-growing large-scale instabilities. Toth and Kalnay (1997) argued from an atmospheric weather perspective that the bred vectors are stochastically and non-linearly modified versions of the leading Lyapunov vector (LLV) i.e. Lyapunov vectors grow from an initial perturbation with infinitesimal amplitude and are evolved for a quasi-infinite time (global), they have linear growth and are tangent linear to the chaotic attractor.

Toth and Kalnay (1997) also showed that very small amplitude initial random perturbations growing on tropospheric flows will, after an initial transient period (about a week or so), converge on the structure of the LLV. BVs on the other hand are finite amplitude, finite time (local) and for our purposes will be typically constructed to be in the nonlinear evolution regime (Pazó et al., 2010). The breeding method is based on the procedure used to calculate the Lyapunov vectors and its ease of implementation makes it readily applicable to nonlinear geophysical models with complex physical parameterization schemes.

In the bred vector method the perturbations are periodically rescaled using a global (or regional) scaling factor which will for our application typically be chosen so that they approximate fast-growing errors within the period of a typical OceanMAPS data assimilation cycle. The choice of initial perturbation amplitude and period between rescaling sets the spatio-temporal scales of interest, thus the BV approach potentially allows one to focus on dynamical instabilities with a range of growth rates and saturation amplitudes.

The approach we have outlined readily allows our ensemble to be initialized about a control analysis from data assimilation but to contain, by construction, information about the evolving flow dependent growing errors. Thus it is reasonable to assume that the bred vectors structures should often be found in regions where forecast errors are large.

3.4.1. Ensemble initialization

In our study of the EAC we wish to excite processes associated with baroclinic instabilities (i.e. eddy formation) with error growth rates and structures appropriate to the control analysis errors over a 7 day data assimilation window. In order to locate where the dominant EAC instabilities arise we perturbed the model initial temperature T at all vertical levels with a small uniformly distributed uncorrelated perturbation and integrate forward for several days repeating this procedure at 7 day intervals over the 6 month period. The error growth rate (i.e. the ratio between the initial and evolved RMS error) was calculated at each vertical level and the response to the perturbation noted. In nearly all cases the largest response was found to be at, or close to, the 250 m level i.e. centered at or close to the thermocline. This is consistent with observational studies of baroclinic instabilities in the EAC (Ridgway and Godfrey, 1997). Further tests examined a variety of approaches to initializing the ensemble, ranging from perturbing SLA (as in Miyazawa et al. (2005), Yin and Oey (2007)) to perturbing SST only. These exploratory tests identified introducing a small uniform random spatially uncorrelated perturbation to temperature T at all vertical levels to be an effective means of ensemble initialization prior to breeding with subsequent rescaling against RMS error at T250. A close relationship was observed between the BV spatial patterns of T,S and SLA (not shown) suggesting that rescaling against RMS errors in salinity at 250 m or SLA would be equally effective choice of norms. The critical point is to measure error growth at the thermocline. Equilibrated BVs were found to be relatively insensitive to initial disturbances whether they be random or weekly anomalies.

3.4.2. Growth rates and rescaling parameters

The procedure for computing n bred vectors is as follows.

1. First we add n random fields to the analysis temperature fields at all levels. In practice we apply a small uniformly distributed random perturbation to T at all horizontal grid points and at all vertical levels so that the perturbed field is given by $T_n^p(t_0) = T^a(t_0) + \delta T_n$ where p denotes perturbation, a analysis, t_0 is the initial time and where δT is a 3-dimensional field of spatially uncorrelated random numbers.
2. Next the model is integrated forward for $\delta t = 7$ days for n perturbed fields and for an additional unperturbed control forecast $T^c(t_0) = T^a(t_0)$.
3. After integration, the difference between the n perturbed forecasts $T_n^p(t_0 + \delta t)$ and the control forecast $T^f(t_0 + \delta t)$ are calculated and scaled using the L2 or Euclidean norm. Specifically the rescaling factor f_n is determined as the ratio of initial anomaly RMS over evolved anomaly RMS at T250 for each n perturbed forecasts. This rescaling factor is now applied globally to all perturbation fields and at all model levels, for all prognostic variables. We now have n perturbation vectors P_n for each field $F_{i=1,\ldots,5} \in (\eta, T, S, u, v)$

$$P_n(F_{i_n}, t_0 + \delta t) = f_n(t_0 + \delta t)(F_{i_n}^p(t_0 + \delta t) - F_i^f(t_0 + \delta t)) \qquad (1)$$

   where superscripts p and f denote perturbation and forecast respectively.
4. The n rescaled perturbation vectors are now added to the current analysis provided by the EnOI data assimilation system and the new ensemble is integrated forward.

5. Repeat step 2 noting that we now have n perturbed fields for (η, T, S, u, v) and steps 3 and 4.

After an initial transient period ($N \approx 10$ cycles) clearly defined growing perturbation vector structures develop. Now we define the initial bred vectors after N cycles at time $t = t_0 + N\delta t$ to be the rescaled perturbation vectors Eq. (1) while the evolved bred vectors are the evolved unscaled perturbation vectors

$$P_n(F_{i_n}, t_0 + N\delta t) = (F^p_{i_n}(t_0 + N\delta t) - F^f_i(t_0 + N\delta t)) \quad (2)$$

after 7 days integration. In our experiments we consider a maximum of $n = 12$ ensemble members. As in Corazza et al. (2003), we take the growth over an analysis period (7 days) to be the inverse of the bred vector rescaling parameter at the analysis time. We have chosen to use the ensemble average of the individual BVs as a means for determining regions that remain coherent and relatively non-dispersive over finite periods of time; we will refer to these as regions where BVs are coincident. In the subsequent results and discussion sections we take the difference between the day 7 control (unperturbed) forecast and the verifying analysis to be the control forecast error. Also considered were paired BVs, where for each respective initial BV a perturbation vector of opposite sign was also added such that the ensemble average of the initial perturbation vectors was identically zero. Little qualitative difference was found between paired and un-paired BVs.

3.5. Discussion

Predictability is associated with the stability of the flow with respect to perturbations (errors) and their associated growth. For infinitesimal initial perturbations error growth may be close to linear and the growing perturbations may be well described using a tangent linear approximation to the full non-linear evolution equations. In such cases SVs i.e. the perturbations with the greatest linear growth over a specified time interval, for a given norm and defined over a specified target area, are appropriate. However, in predictability studies of strongly nonlinear systems linear growth is seen over only an initial small fraction of the predictability time, hence what is more relevant to predictability than the leading Lyapunov exponent is the evolution of finite size perturbations under the full non-linear equations. Moreover, it is often the case that for a given norm some perturbations with given spatial structures may rapidly amplify whereas others will grow more slowly or even decay. That is perturbations that are well embedded on the chaotic attractor will grow whereas those that are not will decay.

The chaotic attractor of a nonlinear system is a zero volume structure of typically fractal dimension (less than the dimension of phase space) and is built from the remote past through a stretching-and-folding mechanism common to globally bounded chaotic dissipative systems possessing at least one Lyapunov exponent greater than zero (Kalnay, 2003). While singular vectors correspond to the disturbance that yields the largest linear growth over a specified time interval they are often not well embedded in the attractor. Perturbation vectors that contain by construction information from the past i.e. have evolved within the flow, such as bred vectors and finite time normal modes will by construction have the advantage of being well adapted to the attractor. Vectors using only information about the future, such as SVs cannot be expected to reflect the geometry of the attractor. Pazó et al. (2010) showed that perturbations initialized as SVs have been found to lead to strongly correlated perturbations at large-scales thereby implying a low degree of diversity. Such methods require additional methods to construct a proper and diverse ensemble, for example mixed initial and evolved SVs or rotated SVs (Molteni et al., 1996).

Ensemble prediction methods may be deterministic, such as those based on rescaling i.e. bred vectors or the so called square root ensemble Kalman filter family, or stochastic (ensemble Kalman filter with perturbed observations). In large scale atmospheric applications on synoptic timescales an extended period of linear error growth is often observed. In such cases it is not uncommon for all types of perturbation vectors (finite and infinitesimal) to show a tendency to converge to the leading Lyapunov vector with the consequence that ensemble diversity is greatly reduced. In response alternative approaches that combine aspects of both deterministic and stochastic methods have been demonstrated by O'Kane and Frederiksen (2008a), whereby bred perturbation vectors are used to project onto fast growing large scale atmospheric disturbances associated with mid-latitude regime transitions complemented by stochastic forcing of the small scales representative of subgrid scale stochastic processes. Recently the ensemble transform Kalman filter in conjunction with small scale stochastic forcing has been applied in operational ensemble numerical weather prediction (Bowler et al., 2009; O'Kane et al., 2008). This methodology produces perturbations that are closely related to BVs but periodically orthogonalized (see Bowler et al., 2009). For the EAC, and presumably for highly non-linear flows dominated by large eddy variability, we have found that bred perturbation vectors do not show a tendency to collapse onto the LLV but instead remain globally diverse. In such cases, and in contrast to typical atmospheric applications, BVs are inherently norm dependent, finite time, nonlinear generalizations of Lyapunov vectors.

Ensemble prediction methods, such as those developed for NWP have only very recently been applied to explore the dynamics and predictability of oceanic flows, however their applicability to WBCs seems a natural choice. Miyazawa et al. (2005) used BVs in an ensemble forecast experiment (using 10 members) of the Kuroshio meander, successfully predicting the meander position with a lead time of 60 days. Fujii et al. (2008) also studied the Kuroshio but using singular vectors (SVs).

Yin and Oey (2007) applied the BV method (using 20 members) to a case study of an eddy shedding event in the Gulf of Mexico (2006). Both (Miyazawa et al., 2005 and Yin and Oey, 2007) perturb and rescale by SLA and assimilate only a limited set of observations. Our approach differs from that previously applied to Northern Hemisphere WBCs (Miyazawa et al., 2005; Yin and Oey, 2007) in that we assimilate SLA from altimetry, temperature and salinity profile observations from XBT, CTD and Argo, and AMSRE SST and rescale against T250 (throughout and for convenience we take T250 to mean temperature at 254.86 m) rather than SLA. Our motivation for doing this is that by rescaling against T250 we directly sample from the region of dominant instability, the thermocline, at the spatio-temporal scales of interest.

An alternative approach can be found in a case study of the Gulf of Mexico by Counillon and Bertino (2009) who employed a novel approach to rescale variances of forecast error in an EnOI data assimilation scheme combined with stochastic perturbation of the lateral and atmospheric boundary conditions. EnOI assumes that the temporal variability is representative of the instantaneous forecast errors, or alternately that a climatology of errors in which no flow dependency or errors of the day are present, can be a reasonable representation of the instantaneous forecast error. Counillon and Bertino (2009) showed promising results using a 10 member ensemble with a 7 day forecast horizon.

Although a standard approach in operational NWP finite amplitude dynamically generated perturbation vectors such as those produced by BVs, ET and ETKF methods are not used in current operational ocean forecasting systems. Indeed the aforementioned EPS studies encompass nearly the entirety of the published

literature as pertinent to the oceans. To-date there has been no discussion about how, or if, bred vector structures relate to forecast errors, and if so does the possibility exist to generate background error covariances based on flow dependent errors of the day in ocean data assimilation. We examine these issues in the following results section.

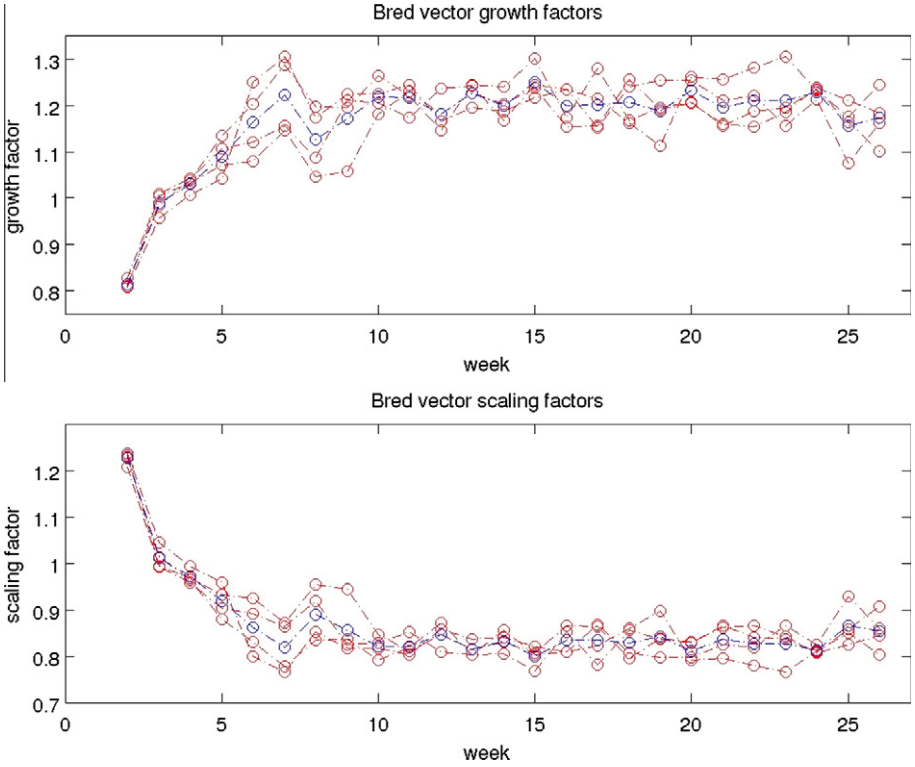

Fig. 2. Top) bred vector growth and bottom) rescaling factors beginning 20th November 2007 through to 13th May 2008 for 4 BVs (red) and their average (blue). (For interpretation of the references to color in this figure legend, the reader is referred to the web version of this article.)

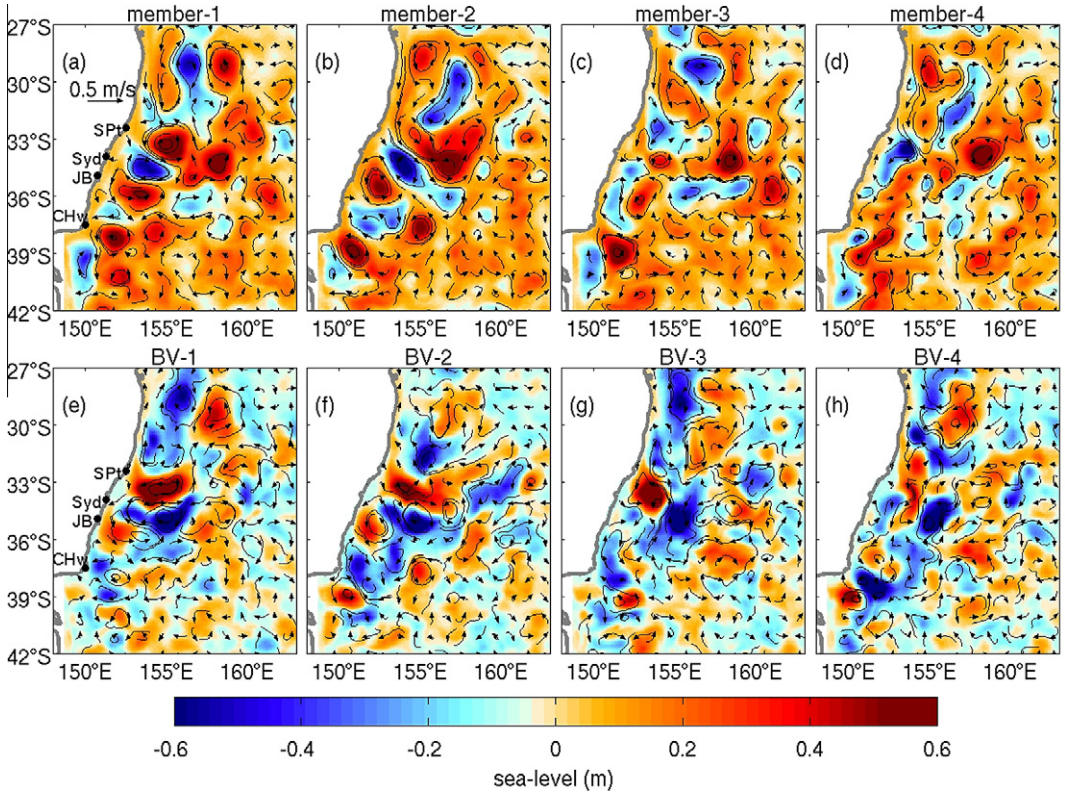

Fig. 3. Surface height on T cells. Row 1 (a)–(d); day 7 ensemble forecasts valid for the 18th March 2008. Row 2 (e)–(h); corresponding evolved bred vectors on day 7. Velocity vector field has been overlaid. Evolved bred vectors correspond to the difference between control and perturbed forecast after 7 days.

4. Results

Our primary aim is to examine the structure of bred vectors and their relation to forecast errors (forecast minus verifying analysis) over a typical 7 day forecast period. We compute a total of 12 perturbed ensemble members. However, due to the high cost of operational systems, we are particularly motivated to explore the information content of smaller ensembles. Further we note that (Tracton and Kalnay, 1993) (see also Toth and Kalnay, 1997) implemented the first operational BV EPS for NWP at the National Meteorological Center (NMC) using a 4 member ensemble.

In Fig. 2 we compare (top) bred vector growth rates and (bottom) bred vector rescaling factors over the entire 25 week period considered including the spin-up period. We find that from initialization with random perturbations to development of well organized spatial structures the spin-up period for bred vectors development in the EAC is 10 cycles. This is similar to the typically 3–5 days (6–10 cycles) period observed in ensemble NWP studies (O'Kane et al., 2008). We also find that the rescaling factor is >1 over the first 4 weeks and it is only after the instability structures are sufficiently coherent that growth (i.e. rescaling factor < 1) occurs. This result, similar to that observed by Yin and Oey (2007), reflects the tendency of the model to damp random perturbations (this effect is related to dissipation operator as discussed by Griffies and Hallberg (2000)). The results in Fig. 2 are for 4 independent bred vectors and the ensemble average. The rescaling factor asymptotes to ≈0.85 corresponding to an average growth factor of ≈1.17 over 7 days. As stated previously the rescaling factors are calculated for the entire domain.

Recalling that the initial (t_0) perturbations are uncorrelated noise, the evolved bred vectors have spatially coherent structures that resemble anomalies associated with eddies (Toth and Kalnay, 1997). For chaotic systems the linear long term growth rate of any random perturbation converges to the first Lyapunov exponent and

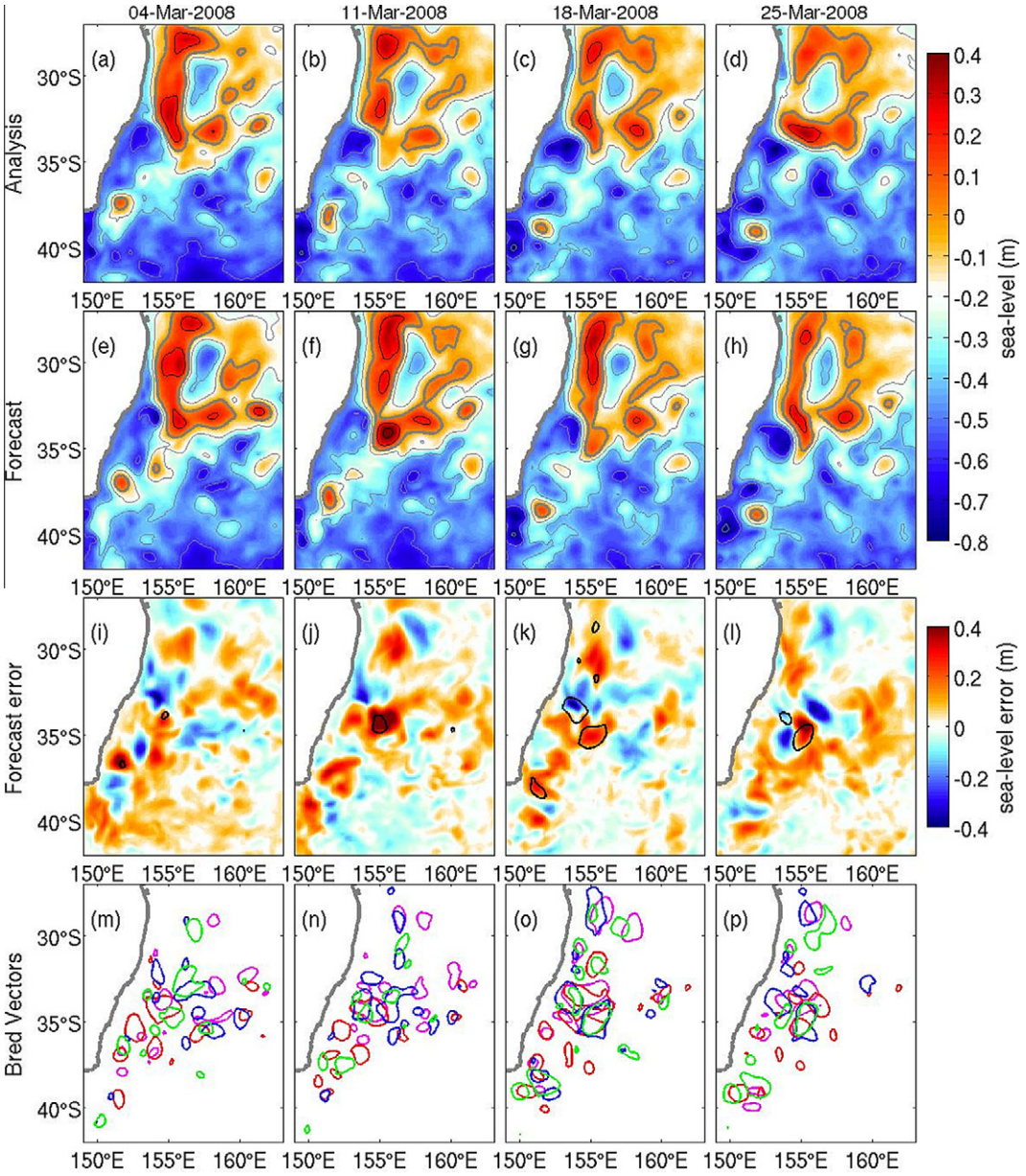

Fig. 4. Surface height on T cells. Columns 1–4 depict results valid for the 4th, 11th, 18th and 25th March 2008 respectively. Row 1 (a)–(d); Analysis fields, Row 2 (e)–(h); 7 days control forecasts. Row 3 (i)–(l); Comparison of ensemble averaged (4 members) bred vectors (±0.35 m contours) and day 7 forecast error (shaded) valid for the (i) 4th; (j) 11th; (k) 18th and (l) 25th March 2008. Row 4 (m)–(p); ±0.35 m contours for each of the 4 individual bred vectors.

the LLV is the vector to which, given sufficient time, all random perturbations will converge (Kalnay, 2003). Because the method of calculating BVs is an extension of that used to calculate the first Lyapunov exponent one might expect all bred vectors to converge to the LLV. However, when attempting to forecast complex systems where multiple instabilities coexist we are interested in the finite time or local spatio temporal stability properties of the flow rather than the long term or global properties. In Fig. 3, we show SLA and surface velocity components of the 7 day perturbed forecasts valid for the 18th March 2008 for 4 ensemble members. Also shown in Fig. 3 (row 2) are the SLA and velocity components of the associated BVs. We clearly see that the BVs are globally distinct, but note some common features including a large amplitude coherent structure in the area offshore from SPt and Cape Howe (CH: 37.50°; 149.97°E). These features are indicative of localized areas of instability.

For the EAC we are interested in where the BVs are coincident as determined by coherent regions where local instabilities are dominant. We determine these regions of coincidence by taking the ensemble average of the BVs. In Fig. 4 (rows 1 and 2) we show the verifying analysis (from the current DA cycle) and the 7 day forecast valid for the same date. In (rows 3 and 4) an ensemble average of 4 evolved (day 7) BVs are compared to the control forecast error (row 3; shaded) for sea level for 4 successive 7 days periods beginning on the 26th February 2008 and valid on the 4th, 11th, 18th and 25th of March. Having identified local regions of instability through ensemble averaging of the individual BVs we are interested to see if these areas correspond to regions of large

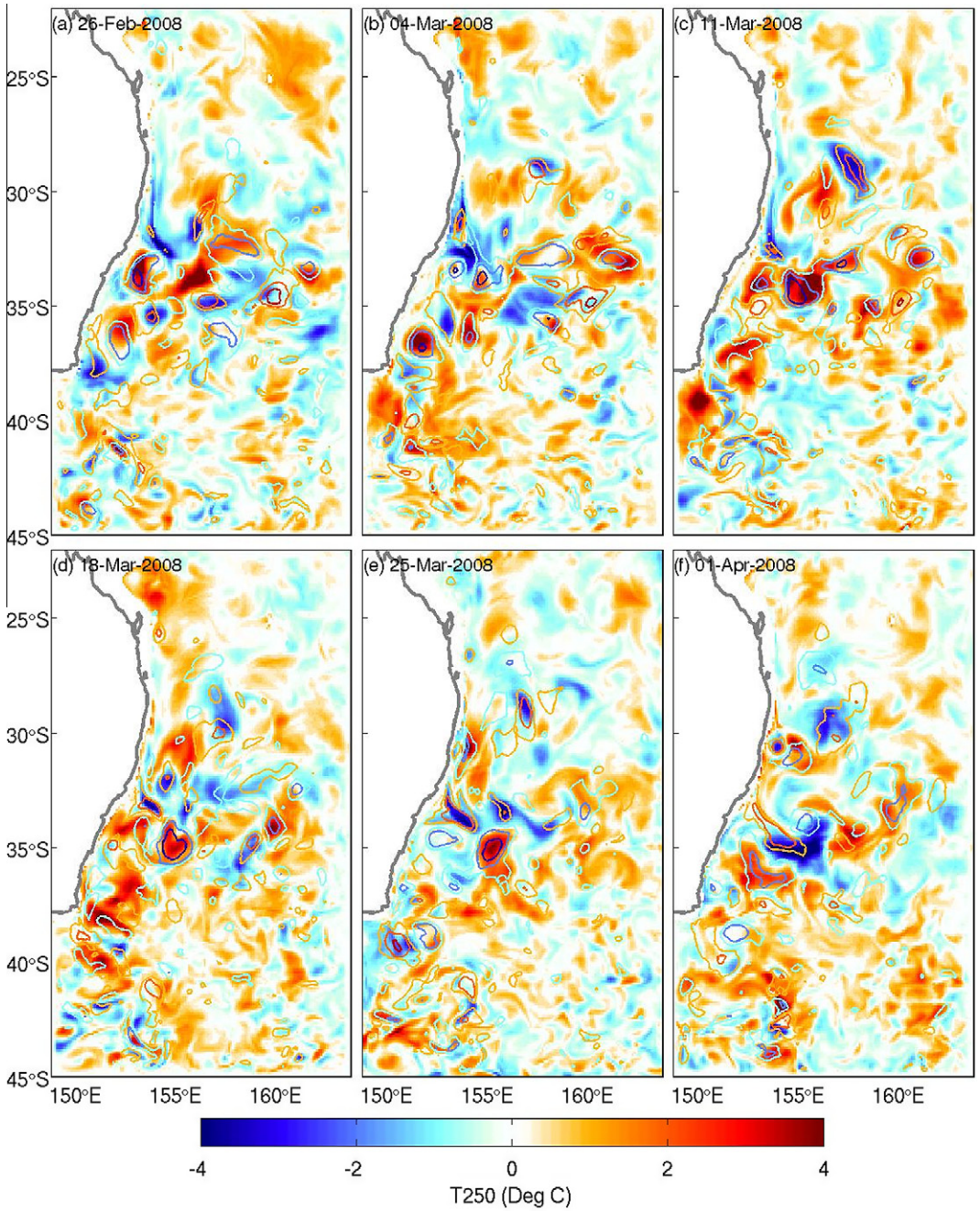

Fig. 5. Comparison of ensemble averaged evolved bred vectors (4 members contours) and forecast error (shaded) for T250 at weekly intervals over a 6 weeks period beginning on the 26th February 2008. Contours shown are ±3.5 °C, ±2.0 °C and ±1.0 °C.

forecast error. Fig. 4 (row 4) shows individual BVs (red, blue, green, magenta) at the 0.35 m η contour (chosen for clarity). The corresponding ensemble average has been superimposed on the forecast errors (Fig. 4 row 3, black contours). The individual BVs illustrate the inherent instability of the EAC. It is clear that the ensemble averaged BV structures are in regions corresponding to the dominant dynamic instabilities centered offshore of SPt (32.5°S), Jervis Bay (35°S), Merimbula (36.90°S) and Cape Howe (37.50°S). These regions, associated with the Tasman Front and the EAC extension, also correspond to the areas of the largest forecast errors.

The evolving BVs and their corresponding growth factors (Fig. 2) describe the growth and decay of dynamic instabilities and areas of large forecast uncertainty. Clearly 7 day forecast errors are dominated by the eddy variability of the EAC and the coherent areas of large forecast error associated with fast growing instabilities appear to be captured by the BVs. The EAC exhibits constantly evolving instabilities that undergo rapid growth and decay cycles. These instabilities are associated with eddy variability in a band extending East between 32° and 35°S. This behavior can be seen in the evolution of the BV averages in Figs. 5 and 6 where we examine T250 over a 12 week period beginning 26th January 2008. These figures show the evolved BVs at day 7, showing the ±3.5, ±2.0 and ±1.0 contours, and the forecast error (color). Figs. 5 and 6 further demonstrate the close correspondence and anti-correlation of the ensemble averaged BV structures to the forecast errors over the entire 3 month period shown. The correspondence between the ensemble averaged BVs and the forecast error is often quite remarkable. Consider for e.g. 11th March (Fig. 5(c)). This shows several fairly localized areas of large forecast error including the negative errors (blue filaments) around 34°S

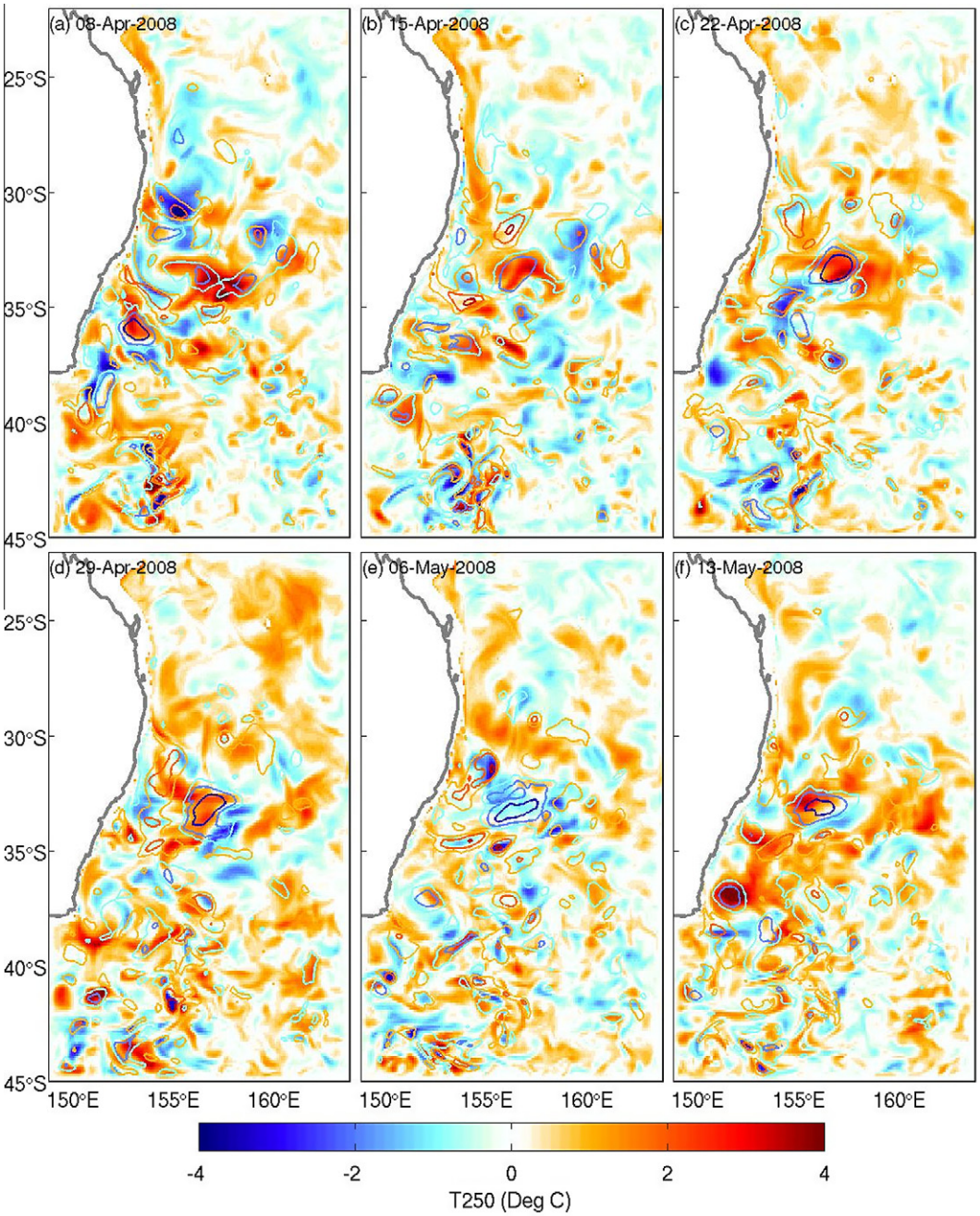

Fig. 6. As for Fig. 5 but for the 6 weeks period beginning on the 8th April 2008. Contours shown are ±3.5 °C, ±2.0 °C and ±1.0 °C.

plus a large positive forecast error around 35°S. These errors are well predicted by the BV ensemble average, with similarly shaped co-located perturbations of opposite sign in those regions. The forecast errors and BVs are not always coincident, but sometimes, even the small scale, relatively noisy, forecast errors are well represented by the BVs (e.g. Fig. 5(f), 155°E and South of 40°S). These results imply that the largest 7 day control forecast errors arise due to instability processes associated with the intrinsic variability of the EAC. Further, we find that the BVs generally do an excellent job of representing these instabilities.

A measure of the nonlinearity may be made by estimating the Rossby number (Fig. 7) as the relative vorticity averaged over 0–200 m divided by the absolute value of the Coriolis parameter. We do this for the control and two perturbed forecasts valid on the 18th March. The corresponding divergence fields are shown in Fig. 8. In both Figs. 7 and 8 the area of largest horizontal gradients occurs near the separation region close to SPt and in an area of large positive vorticity south of Cape Howe. These regions have not only correspondingly large BV structures (Fig. 5) but also are regions of large forecast error. During the period 1st–15th April (Fig. 5(f) and Fig. 6(a) and (b)) we note a region of large forecast error, with corresponding BV structures, off the east coast of Tasmania between 41 and 44.5°S and centered on 153.5°E. These features are associated, not with the dominant branch of the EAC, but with a weaker southward extension of the current to higher latitudes and the development of a pair of cold core (43.5°S, 152.5°E)/warm core

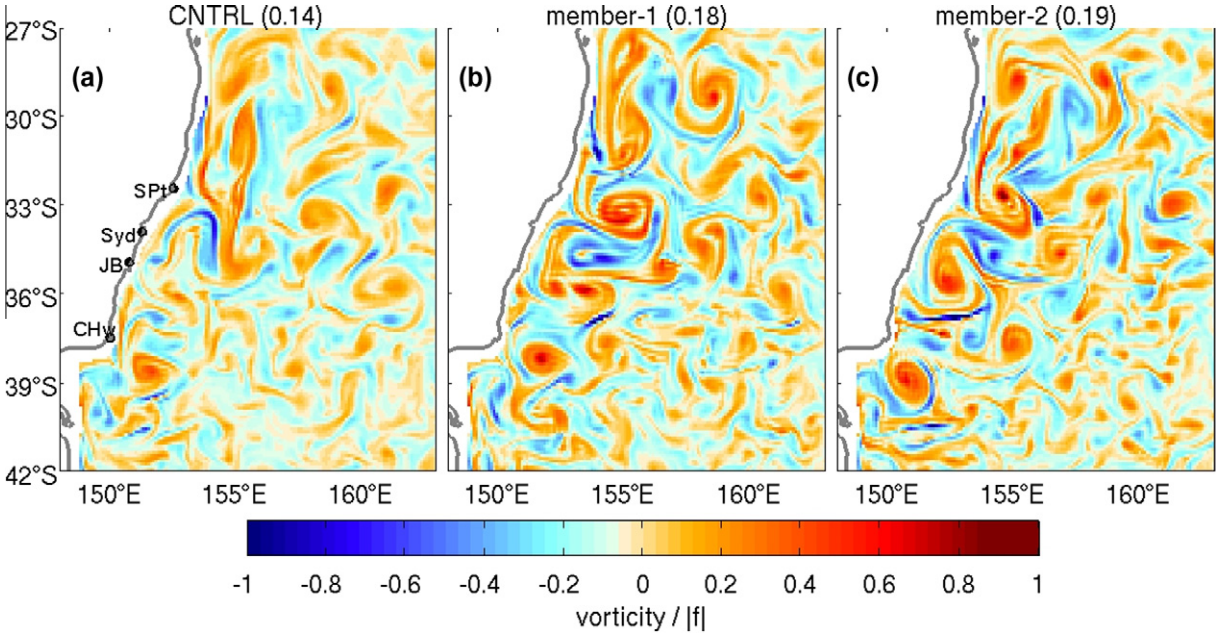

Fig. 7. Rossby number for 7 days forecasts valid for the 18th March 2008. (a) control forecast, (b) and (c) individual perturbed forecasts.

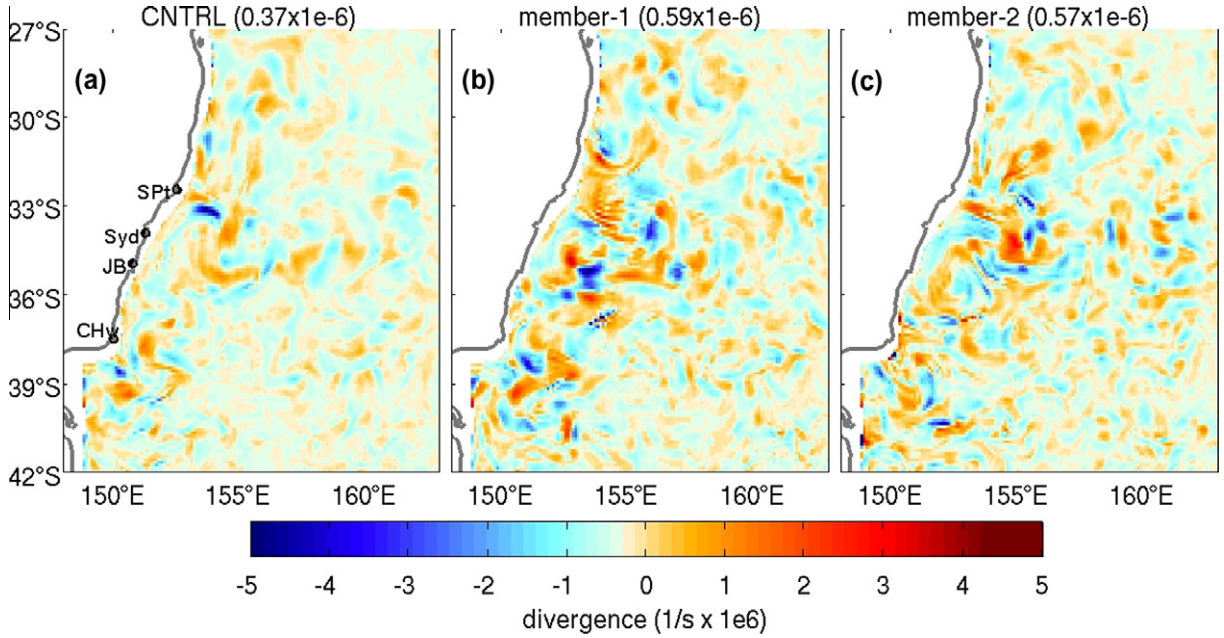

Fig. 8. The divergence for 7 days forecasts valid for the 18th March 2008. (a) control forecast, (b) and (c) individual perturbed forecasts.

(42°S, 153.5°E) SLAs that persisted through this period (for details see www.marine.csiro.au/remotesensing/oceancurrents/SE).

More generally, during this period, a series of alternating warm and cold core SLAs formed along the east coast for latitudes below 30°S. The positions of these SLAs are associated with large forecast errors and are closely reflected by the positions of the BV structures at T250 (Fig. 5(f) and Fig. 6(a) and (b)).

In contrast to the control forecast (Figs. 7 and 8(a)) the perturbed forecasts (Figs. 7 and 8(b) and (c)) display markedly increased regions of nonlinearity and divergence. The area averaged Rossby

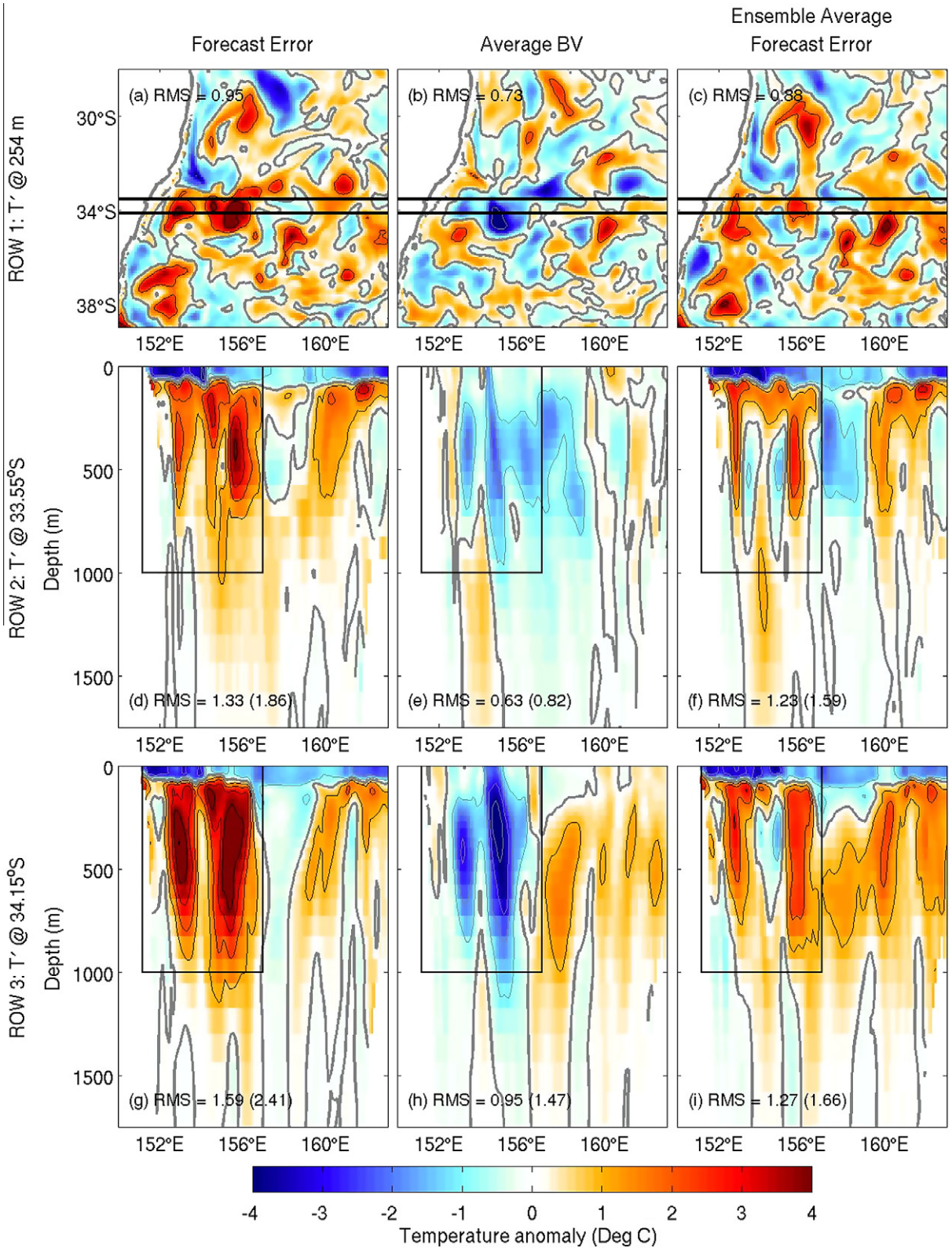

Fig. 9. Comparison of day 7 forecast error (left), ensemble averaged bred vectors (middle) and ensemble averaged forecast error (right) (4 members) valid on the 11th March; Showing T250 (a)–(c) and vertical sections along 33.55°S (d)–(f) and 34.15°S (g)–(i). RMS errors are shown for the entire domain and for subdomains (in brackets) encompassing the dominant coherent error structures.

number and divergence are 0.14 and 0.37 $\times 10^{-6}$ s^{-1} in the control and greater than 0.18 and 0.57 $\times 10^{-6}$ s^{-1} in the perturbed runs. We interpret this as evidence that individual BVs are more able to capture areas of enhanced instability.

We next examine T250 and through the water column in vertical sections (Figs. 9–11). We focus on a three week period, 11th, 18th and 25th March, when both large coherent forecast error and BV structures formed, centered on 34°S; 156°E. This period corresponds to the growth of a cold core eddy to the southeast of SPt. In Fig. 9 we see the dominant local forecast error centered on 34°S, 154°5′E occurring on the 11th March in vertical sections along 33°55′S (offset from the anomaly) and 34°15′S (centered

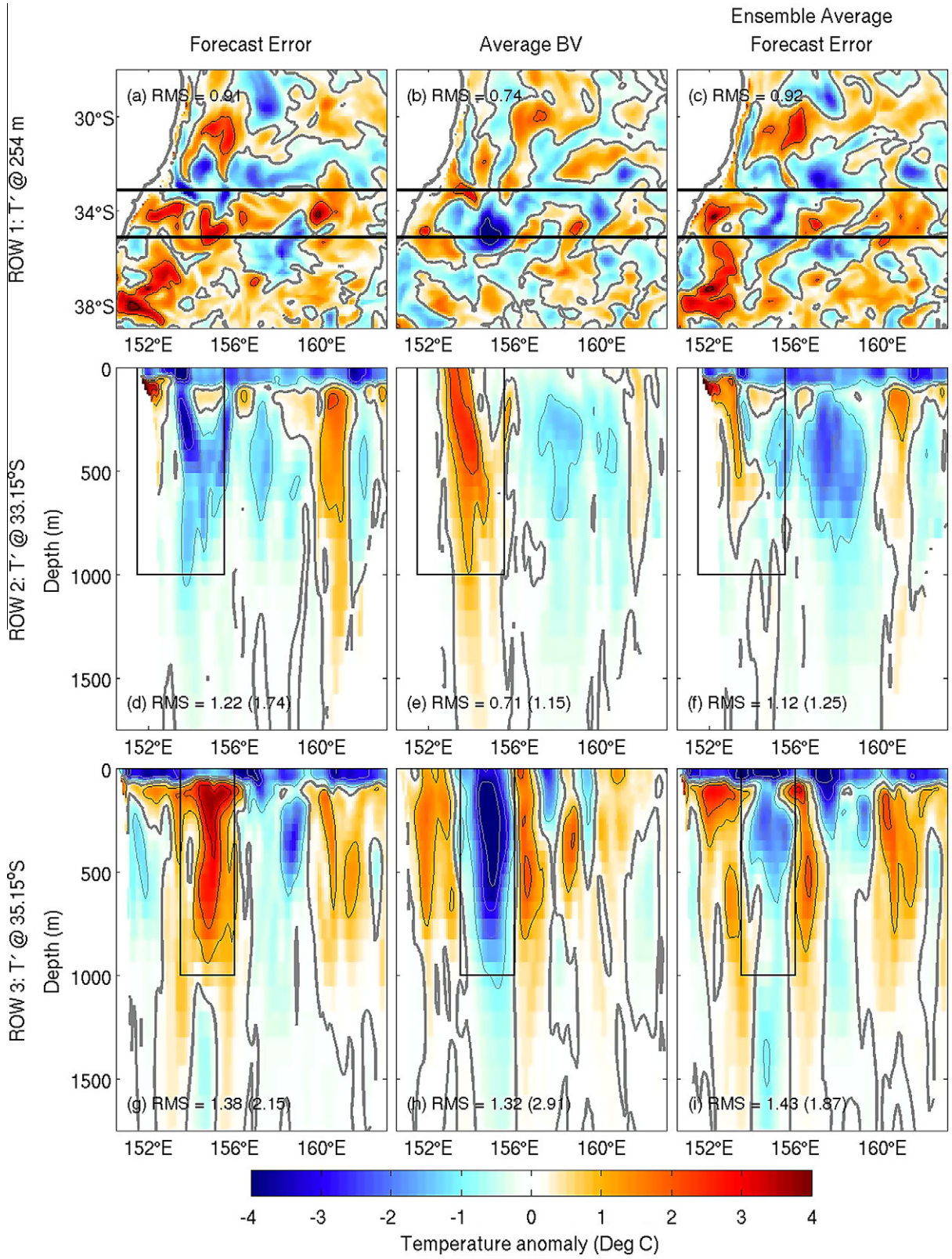

Fig. 10. As for Fig. 9 but on 18th March and for sections along 33.15°S (d)–(f) and 35.15°S (g)–(i).

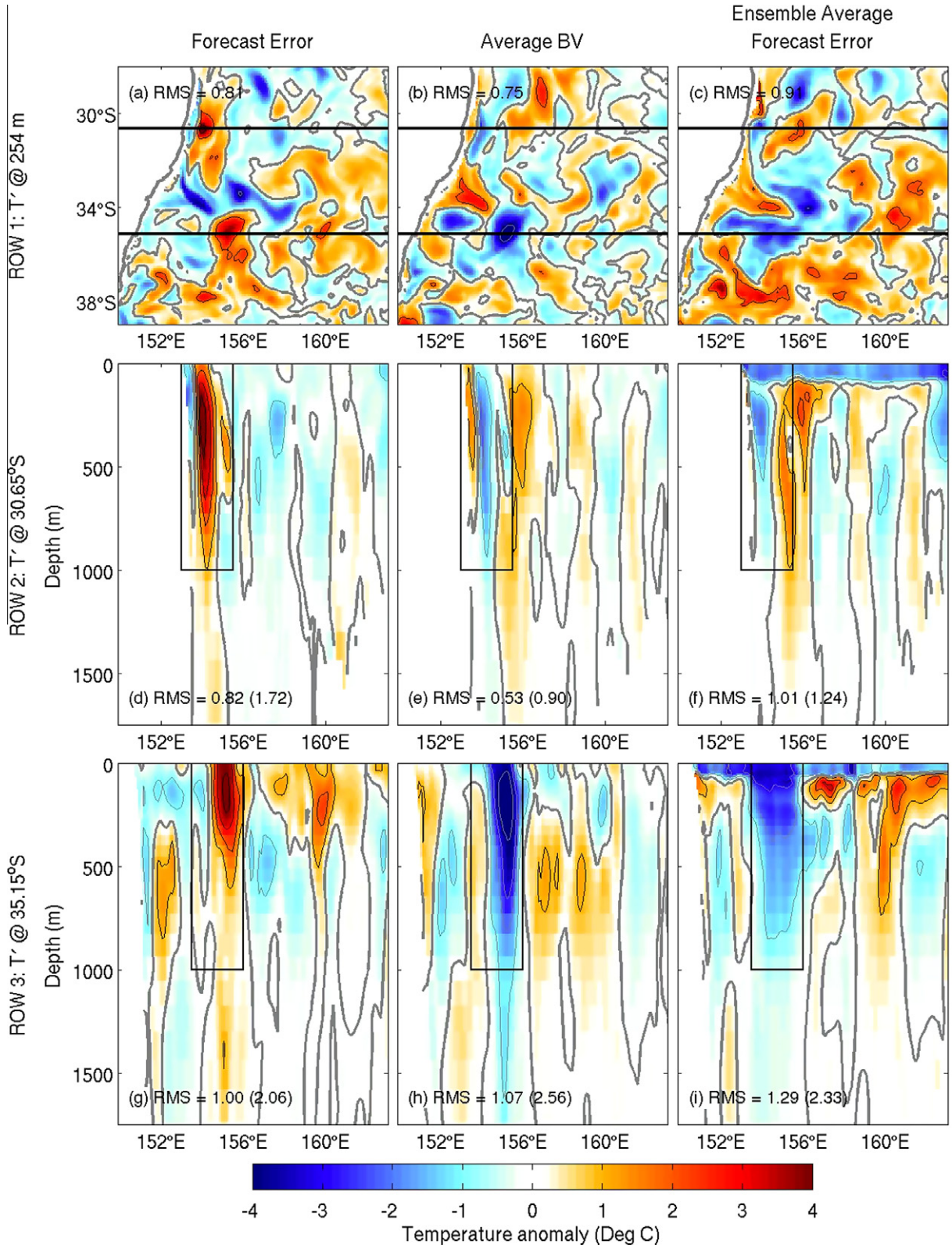

Fig. 11. As for Fig. 9 but on 25th March and for sections along 30.65°S (d)–(f) and 35.15°S (g)–(i).

on the anomaly). In these vertical sections we see regions of coincidence between the evolved BV averages and the control forecast errors. In many cases (but not all) these are regions where substantial reductions in the ensemble forecast errors occur and we interpret these to be regions of large dynamic instability. It is clear that the instabilities in the region 151.2°–157°E are centered around 250 m and extend down to 1000 m. It is also evident that the 7 day ensemble forecast errors (4 members) have significantly smaller amplitudes and contracted vertical structures as compared to the control forecast errors. For this case the RMS scores for the 4

Table 1
Day 7 control versus ensemble forecast RMS errors 11th–25th March 2008 corresponding to the domains shown in Figs. 9–11. RMS errors are shown for the entire domain and for the subdomains (in brackets) encompassing the dominant coherent error structures.

Forecast RMS				
	Control	BV average (4)	BV average (8)	BV average (12)
11th March T (250 m)	0.95	0.88	0.87	0.88
18th March T (250 m)	0.91	0.92	0.90	0.88
25th March T (250 m)	0.81	0.91	0.94	0.84
11th March 34.15°S	1.59(2.41)	1.27(1.66)	1.29(1.71)	1.29(1.64)
18th March 35.15°S	1.38(2.15)	1.43(1.87)	1.37(1.59)	1.33(1.65)
25th March 35.15°S	1.00(2.06)	1.29(2.33)	1.20(1.69)	1.22(1.90)
11th March 33.55°S	1.33(1.86)	1.23(1.59)	1.20(1.61)	1.22(1.58)
18th March 33.15°S	1.22(1.74)	1.12(1.25)	1.17(1.39)	1.14(1.25)
25th March 30.65°S	0.82(1.72)	1.01(1.24)	1.03(1.25)	0.95(1.19)

member ensemble forecast are noticeably better than the control and that increased ensemble size (up to 12 members) resulted in only modest reductions in RMS errors (see Table 1). In this case the ensemble forecast outperforms the single control.

In Figs. 10 and 11 and Table 1 we contrast BV and ensemble forecast error averages for 4, 8 and 12 member ensembles with the control forecast valid on the 18th and 25th March respectively. As we have initialized the control forecast with an analysis on the 11th March information about the strengthening cold core eddy is now represented in the analysis and we expect the subsequent 7 day control forecast errors to be smaller. In addition as we are perturbing about the analysis we should also see corresponding reductions in the magnitude and spatial extent of coherent regions of large forecast error and associated BVs. This is evident in Figs. 10 and 11(g) and (h), respectively for vertical sections along 35°15′S where we see the vertical extent of the coherent feature in the inner box is successively reduced from 1000 m (Fig. 9(g) and (h)) to 750 m and 500 m, respectively. One also expects that where the dominant regions of forecast error are not due to dynamic instability then larger ensembles may be required for improved forecasts. This was found to be the case in RMS scores for T at 250 m (Table 1). In these cases, while only 4 members were needed to identify regions of large forecast uncertainty due to dynamic instability, we required increased ensemble size in order to get comparable RMS scores over the period during which the dominant instabilities decay. This point is illustrated in Table 1 where RMS scores for control forecasts are compared to those from ensemble averaged forecasts (4, 8 and 12 members) on the 11th, 18th and 25th March 2008 with domains corresponding to those shown in Figs. 9–11, respectively.

In Figs. 10 and 11 we also focus on smaller forecast error structures along 33.15° and 30.65°, respectively. In the region 33.15°S; 151.5–155.5°E, Fig. 10(d) and (e) we see a coherent cold forecast error structure extending down to 500 m with maximum near 250 m and a corresponding warm BV structure. We also note in Fig. 11(a) for the T250 there occurs a localized region of large forecast errors close to the coast centered along ≈30.65°S and that although the associated BV structure (Fig. 11(b)) is relatively weak, the ensemble forecast (Fig. 11(c)) is substantially improved in this region.

The results presented demonstrate that the coherent structures we have identified through taking ensemble averages of the respective BVs tend to anti-correlate with regions of large forecast errors. We also find that these highly localized error structures, while typically associated with the Tasman Front and the EAC extension, may also occur in any area where dynamic instabilities are expected to be the dominant processes. Moreover our results demonstrate that these dynamic instabilities are generated at or near the thermocline and are therefore most likely baroclinic in nature.

5. Discussion

Because BVs are generated in regions of dynamic instability large coherent BV structures, indicative of regions of likely large forecast errors, are typically found to be associated with the emergence of eddies and meanders. We find that over 7 days, dynamic instabilities in the EAC originate at around 250 m and that the largest instabilities are typically located off SPt.

The EAC is inherently unpredictable because it has large eddy variability with a wide range of spatio-temporal scales of interest, therefore representing a severe test of any EPS. We find that forecast errors may be large over 7 days and that, in contrast to a control forecast, BV perturbed forecasts tend to be more strongly nonlinear, with corresponding regions of large divergence. This is because BVs, by construction, contain information about the flow dynamics. BV perturbed forecasts have also been shown to exclude large forecast errors in areas of large dynamic instability and that very few ensemble members are required to qualitatively predict areas of large forecast error. However our results also show that where rapidly growing dynamic instabilities are not present, eddy variability is in a sense more random, and therefore less inherently predictable, many realizations of a forecast may be required to reduce sampling error to the point where the ensemble forecast is useful. This is illustrated in the results of Figs. 5 and 9, 10, 11 where we see a large coherent forecast error structure centered about 34.15°S:151.5–156.5°E on the 11th March that grows in less than a week but decayed over more than 2 weeks. In the rapid amplification phase we see that only 4 bred vector members are required to clearly identify the forecast error structure using temperature. However during the subsequent decay phase, although we could still identify the diminishing coherent region we required an increase in the number of realizations to gain improvement in the ensemble forecast. In general BV structures are associated with regions of the EAC where eddy variability is significant and the current is well defined. A particular example is shown for the period 1st–15th April where the EAC extended along the east coast of Tasmania. For this period large forecast errors and BV structures are associated with the EAC extension to higher latitudes.

The motivation for this study is the representation, or prediction, of regions of large forecast error. In practice, we show that a 4-member ensemble of BVs can predict the regions of largest forecast uncertainty. In some cases, it can even predict regions of small-scale forecast error. Another motivation for BVs is that of adaptive sampling, or targeted observations. Adaptive sampling asks the question: where should additional observations be made to better constrain a forecast? We show that BVs project onto regions of large coherent forecast errors. We speculate that the assimilation of additional observations in those regions would likely improve the subsequent forecast of the ocean state. For example, suppose a glider was deployed at the end of February

in the vicinity of 155°E and 35°S. If observations from such a glider were assimilated, the large forecast error on the 4th March may be reduced. We expect that in the future BVs will prove a useful tool for guiding the adaptive sampling of the ocean.

6. Conclusion

We have conducted an ensemble prediction study of the EAC with a specific focus on the examination of the role of dynamical instabilities and flow dependent forecast errors. We have developed an EPS based on the breeding method to identify the spatial patterns of the fastest growing errors for a given initial state. Here the initial state is an analysis product from the Australian operational ocean forecast system which employs an EnOI DA scheme. We considered a 6 month period spanning the Austral summer and autumn of 2008 corresponding to the seasons of largest eddy variability. We have shown that individual perturbations generated as bred vectors, while globally distinct, can, through ensemble averaging, be used to identify areas of coherence corresponding to regions of large dynamic instability and forecast error. In particular these regions correspond to where the EAC separates from the coast and bifurcates to form the Tasman Front and the EAC extension. Our results show that over 7 days forecast errors arise due to dynamic instabilities and that these forecast errors can be expected to dominate analysis errors. Moreover BVs show some potential to be an effective, computationally inexpensive means to calculate flow dependent background information critical to accurate forecasting. Further a very small BV ensemble may be run to identify regions where additional observations may be targeted.

Acknowledgements

It is a pleasure to thank Dr. Justin Freeman for computational assistance. Financial support for this research is provided by CSIRO, the Bureau of Meteorology, and the Royal Australian Navy as part of the Bluelink project and the US Office of Naval Research (Grant No. N00014-07-1-0422). Satellite altimetry is provided by NASA, NOAA, ESA and CNES. SST observations are provided by NASA, NOAA and Remote Sensing Systems. Argo data were collected and made freely available by the International Argo Project and the national programs that contribute to it (http://www.argo.ucsd.edu, http://argo.jcommops.org).

References

Andrews, J., Scully-Power, P., 1976. The structure of an East Australian Current anticyclonic eddy. J. Phys. Oceanogr. 6, 756–765.
Bowen, M., Wilkin, J., Emery, W., 2005. Variability and forcing of the East Australian Current. J. Geophys. Res. 110, C03019.
Bowler, N., Arribas, A., Mylne, K., Robertson, K., Beare, S., 2009. The MOGREPS short-range ensemble prediction system. Quart. J. Roy. Meteorol. Soc. 134, 703–722.
Brandt, S., 1981. Effects of a warm-core eddy on fish distributions in the Tasman Sea off East Australia. Marine Ecol. 6, 19–33.
Brassington, G., Oke, P., Pugh, T., 2006. Operational Ocean Prediction In Australia, vol. 5. World Scientific Publishing, pp. 87–95 (Chapter 11).
Brassington, G., Pugh, T., Spillman, C., Schultz, E., Beggs, H., Schiller, A., Oke, P., 2007. Development of operational oceanography and servicing in Australia. J. Res. Practice Inform. Technol. 39, 151–164.
Charney, J., 1966. The feasibility of a global observation and analysis experiment. Bull. Am. Meteor. Soc. 47, 200–220.
Corazza, M., Kalnay, E., Patil, D., Yang, S.-C., Morss, R., Cai, M., Szunyogh, I., Hunt, B., Yorke, J., 2003. Use of the breeding technique to estimate the structure of the analysis errors of the day. Nonlinear Proc. Geophys. 10, 233–243.
Counillon, F., Bertino, L., 2009. High-resolution ensemble forecast for the Gulf of Mexico eddies and fronts. Ocean Dyn. 59, 83–95.
Cresswell, G., 1974. Ocean currents measured concurrently on and off the Sydney area continental shelf. Australian J. Marine Freshwater Res. 25, 427–438.
Cresswell, G., 1982. The coalescence of two East Australian Current warm-core eddies. Science 8, 161–164.
Cresswell, G., 1983. Physical evolution of Tasman sea eddy. Australian J. Marine Freshwater Res. 34, 495–513.
Cresswell, G., 1994. Nutrient enrichment of the Sydney continental shelf. Australian J. Marine Freshwater Res. 45, 677–691.
Cummings, J., Bertino, L., Brasseur, P., Fukumori, I., Kamachi, M., Martin, M., Oke, P.R., Testut, C.E., Verron, J., Weaver, A., 2009. Oc ean data assimilation systems for GODAE. Oceanography 22 (3), 96–109.
Evensen, G., 2003. The ensemble Kalman filter: theoretical formulation and practical implementation. Ocean Dyn. 53, 343–367.
Frederiksen, J., O'Kane, T., 2008. Entropy, closures and subgrid modeling. Entropy 10, 635–683.
Fujii, Y., Tsujino, H., Usui, N., Nakano, H., Kamachi, M., 2008. Application of singular vector analysis to the Kuroshio large meander. J. Geophys. Res. 113, C07026.
Gibbs, M., Marchesiello, P., Middleton, J., 1997. Nutrient enrichment of Jervis Bay, Australia, during the massive 1992 coccolithophorid bloom. Marine Freshwater Res. 48, 473–478.
Godfrey, J., Cresswell, G., Golding, T.J., Pearce, A., Boyd, R., 1980. The separation of the East Australian Current. J. Phys. Oceanography 10, 430–440.
Griffies, S., Hallberg, R., 2000. Biharmonic frction with a smagorinsky-like viscosity for use in large-scale eddy-permitting ocean models. Mon. Weath. Rev. 128, 2935–2946.
Griffies, S., Harrison, M., Pacanowski, R., Rosati, A., 2003. A technical guide to MOM4 GFDL, Ocean technical group report No. 5.
Houtekamer, P., Mitchell, H., 1998. Data assimilation using an ensemble Kalman filter. Mon. Weath. Rev. 126, 796–811.
Hurlburt, H., Brassington, G.B., Drillet, Y., Kamachi, M., Benkiran, M., Bourdalle-Badie, R., Chassignet, E.P., Jacobbs, G.A., Galloudec, O.L., Lellouche, J.-M., Metzger, E.J., Oke, P.R., Pugh, T.F., Schiller, A., Smedstad, O.M., Tranchant, B., Tsujino, H., Usui, N., Walcraft, A.J., 2009. High-resolution global and basin-scale ocean analyses and forecasts oceanography. Oceanography 22 (3), 80–97.
Huyer, A., Smith, R.L., Stabeno, P.J., Church, J.A., White, N.J., 1988. Currents off south-eastern Australia: Results from the Australian coastal experiment. Australian J. Marine Freshwater Res. 39, 245–288.
Kalnay, E., 2003. Atmospheric Modelling, Data Assimilation and Predictability. Cambridge University Press.
Kasahara, A., 1972. Simulation experiments for meteorological observing systems for GARP. Bull. Am. Meteor. Soc. 53, 252–264.
Leith, C., 1974. Theoretical skill of Monte Carlo forecasts. Mon. Weath. Rev. 102, 409–418.
Lorenz, E., 1963. Deterministic nonperiodic flow. J. Atmos. Sci. 20, 130–141.
Marchesiello, P., Middleton, J.H., 2000. Modeling the East Australian Current in the Western Tasman Sea. J. Phys. Oceanogr. 30, 2956–2971.
Mata, M., Tomczak, M., Wijffels, S., Church, J., 2000. East Australian Current volume transports at 30S: Estimates from the World Ocean Circulation Experiment hydrographic sections PR11/P6 and the PCM3 current meter array. J. Geophys. Res. 105, 28,509–28,526.
Mata, M., Wijffels, S., Church, J., Tomczak, M., 2006. Eddy shedding and energy conversion in the East Australian Current. J. Geophys. Res. 111, C09034.
Mitchell, H., Houtekamer, P., Pellerin, G., 2002. Ensemble size, balance, and model-error representation in an ensemble Kalman filter. Mon. Weath. Rev. 130, 2791G2808.
Miyazawa, Y., Yamane, S., Guo, X., Yamagata, T., 2005. Ensemble forecast of the Kuroshio meandering. J. Geophys. Res. 110.
Molteni, F., Buizza, R., Palmer, T., Petroliagis, T., 1996. The ECMWF ensemble prediction system: Methodology and validation. Quart. J. Meteor. Soc. 122, 73–119.
Nilsson, C., Cresswell, G.R., 1980. The formation and evolution of East Australian Current warm-core eddies. Progress Oceanogr. 9, 133–183.
O'Kane, T., Frederiksen, J., 2008a. A comparison of statistical dynamical and ensemble prediction methods during blocking. J. Atmos. Sci. 65, 426–447.
O'Kane, T., Frederiksen, J., 2008b. Comparison of statistical dynamical, square root and ensemble Kalman filters. Entropy 10, 684–721.
O'Kane, T., Naughton, M., Xiao, Y., 2008. The Australian community climate and earth system simulator Global and Regional Ensemble Prediction Scheme. ANZIAM J. 50, C385–C398.
Oke, P., Balmaseda, M., Benkiran, M., Cummings, J.A., Dombrowsky, E., Fujii, Y., Guinehut, S., Larnicol, G., Traon, P.-Y.L., Martin, M.J., 2009. Observing system evaluations using GODAE systems. Oceanography, 144–153.
Oke, P., Brassington, G., Griffin, D., Schiller, A., 2008. The Bluelink Ocean Data Assimilation System (BODAS). Ocean Modell. 21, 46–70.
Oke, P., Griffin, D., 2011. The cold-core eddy and strong upwelling off the coast of New South Wales in early 2007. Deep Sea Research 58, 574–591.
Pazó, D., Rodríguez, M., López, J., 2010. Spatio-temporal evolution of perturbations in ensembles initialized by bred, Lyapunov and singular vectors. Tellus 62A, 10–23.
Ridgway, K., Dunn, J., 2003. Mesoscale structure of the mean East Australian Current system and its relationship with topography. Progress Oceanogr. 56, 189–222.
Ridgway, K., Godfrey, J., 1997. Seasonal cycle of the East Australian Current. J. Geophys. Res. 102, 22921–22936.
Roughan, M., Middleton, J., 2002. A comparison of observed upwelling mechanisms off the east coast of Australia. Continental Shelf Res. 22, 2551–2572.
Sandery, P., Brassington, G.B., 2009. Coupled tropical cyclone modelling and adaptive dynamical initialization. CAWCR Technical Report. (017), 50–54.
Sandery, P., Brassington, G.B., Craig, A., Pugh, T.-, 2010. Impacts of ocean-atmosphere coupling on tropical cyclone intensity change and ocean prediction in the Australian region. Mon. Weath. Rev. 138 (6), 2074–2091.
Sandery, P., Brassington, G.B., Freeman, J., 2011. Adaptive nonlinear dynamical initialization. J. Geophys. Res. 116, C01021.

Schiller, A., Oke, P., Brassington, G., Entel, M., Fiedler, R., Griffin, D., Mansbridge, J., 2008. Eddy-resolving ocean circulation in the Asian–Australian region inferred from an ocean reanalysis effort. Progress Oceanogr. 76, 334–365.

Seaman, R., Bourke, W., Steinle, P., Hart, T., Embery, G., Naughton, M., Rikus, L., 1995. Evolution of the Bureau of Meteorology's global assimilation and prediction system. Aust. Met. Mag. 44, 1–18.

Smagorinsky, J., 1969. Problems and promises of deterministic extended range forecasting. Bull. Am. Meteor. Soc. 50, 286–311.

Toth, Z., Kalnay, E., 1993. Ensemble forecasting at NMC. Bull. Am. Meteor. Soc. 74, 2317–2330.

Toth, Z., Kalnay, E., 1997. Ensemble forecasting at NCEP and the breeding method. Mon. Weath. Rev. 125, 3297–3319.

Tracton, M., Kalnay, E., 1993. Operational ensemble prediction at National Meteorological Center: Practical aspects. Weath. Forecasting 8, 379–398.

Tranter, D., Carpenter, D., Leech, G., 1986. The coastal enrichment effect of the East Australian Current eddy field. Deep Sea Research 33, 1705–1728.

Trevisan, A., Pancotti, F., 1998. Periodic orbits, Lyapunov vectors, and singular vectors in the Lorenz system. J. Atmos. Sci. 55, 390–398.

Wei, M., Toth, Z., Wobus, R., Zhu, Y., 2008. Initial perturbations based on the ensemble transform (ET) technique in the NCEP global operational forecast system. Tellus 60A, 62–79.

Wei, M., Toth, Z., Wobus, R., Zhu, Y., Bishop, C., Wang, X., 2006. Ensemble Transform Kalman Filter-based ensemble perturbations in an operational global prediction system at NCEP. Tellus 58A, 28–44.

Wilkin, J., Zhang, W., 2007. Modes of mesoscale sea surface height and temperature variability in the East Australian Current. J. Geophys. Res. 112, C01013.

Yin, X.-Q., Oey, L.-Y., 2007. Bred-ensemble forecast of loop currents and rings. Ocean Modell. 17, 300–326.